

Subfemtosecond Wakefield Injector and Accelerator Based on an Undulating Plasma Bubble Controlled by a Laser Phase

Jihoon Kim,¹ Tianhong Wang¹, Vladimir Khudik,^{1,2} and Gennady Shvets¹

¹*School of Applied and Engineering Physics, Cornell University, Ithaca, New York 14850, USA*

²*Department of Physics and Institute for Fusion Studies, The University of Texas at Austin, Austin, Texas 78712, USA*



(Received 25 April 2021; accepted 16 September 2021; published 12 October 2021)

We demonstrate that a long-propagating plasma bubble executing undulatory motion can be produced in the wake of two copropagating laser pulses: a near-single-cycle injector and a multicycle driver. When the undulation amplitude exceeds the analytically derived threshold, highly localized injections of plasma electrons into the bubble are followed by their long-distance acceleration. While the locations of the injection regions are controlled by the carrier-envelope phase (CEP) of the injector pulse, the monoenergetic spectrum of the accelerated subfemtosecond high-charge electron bunches is shown to be nearly CEP independent.

DOI: 10.1103/PhysRevLett.127.164801

Laser-driven plasma accelerators offer a promising pathway to compact accelerators by sustaining electric fields capable of accelerating a charged particle to GeV energies in less than a centimeter. Furthermore, the plasma can serve as a cathode by supplying the electrons to be trapped and accelerated inside a plasma cavity generated in the wake of an ultraintense laser pulse via time-averaged (ponderomotive) pressure. Such laser-wakefield accelerators (LWFA) [1–3] have produced multi-GeV, low-emittance, ultrashort electron bunches [4–9] without a need for a separate cathode. High-energy electrons generated by LWFAs are promising for various scientific and technological applications from TeV-scale lepton colliders [10] to sources of high brightness radiation and particles [11–16].

Under most circumstances relevant to LWFAs, a phase-averaged (ponderomotive) description of the plasma response to multicycle laser pulses [17] is sufficient to describe their physics, including relativistic self-guiding [3] and the plasma bubble dynamics [18–21]. However, the absolute carrier-envelope phase (CEP) of near-single-cycle (NSC) laser pulses is important for some applications, including ionization injection [22–25] by ultrashort laser pulses [26,27]. Electron injection and acceleration by NSC pulses have also been proposed [28–30] and experimentally demonstrated [31–33] in fully ionized plasmas. However, significant shot-to-shot variation of the electron energy spectrum from CEP slip has been observed [31] for NSC pulses without CEP stabilization. Overall, NSC laser pulses have limited potential as drivers for GeV-scale LWFAs because of their reduced self-focusing [34] results in rapid diffraction and short acceleration distance [28,29,32].

In this Letter, we show that a NSC laser pulse can be harnessed as an ultrafast electron injector when combined with a multicycle higher-intensity laser pulse serving as a long-distance LWFA driver. Using 3D particle-in-cell (PIC)

simulations, we show that asymmetric plasma flow controlled by the CEP of a moderate-power injector pulse induces undulations of a long-lived plasma bubble generated by the driver pulse. When the undulation amplitude exceeds the analytically derived threshold, electron injection by a phase-controlled undulating bubble (PUB) takes place. Unlike some of the injection scenarios mediated by the modulation and evolution of the driver pulse [18,19,35], the PUB-based injection mechanism is fundamentally different in that the driver pulse remains unchanged, and it is the phase of a transient NSC pulse that controls electron injection. This two-pulse approach shown in Fig. 1 turns the key disadvantage of NSC pulses—short propagation in tenuous plasmas—into an advantage: highly localized electron injection. Because most of the energy gain occurs after injection pulse depletion, PUB-injected electrons form subfemtosecond high-current (10's of kAs)

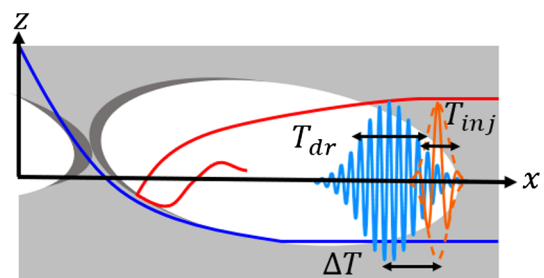


FIG. 1. Schematic of a laser-wakefield accelerator with PUB injection. A transversely undulating plasma bubble driven by the combination of a near-single-cycle injector pulse (orange) and a multicycle driver pulse (light blue) periodically traps electrons from the ambient plasma. Time-dependent injector CEP controls bubble centroid displacement from the propagation axis (dashed line), determining which electrons are injected into (red line) or pass through (blue line) the bubble.

monoenergetic electron bunches with a CEP-independent energy spectrum.

Analytic criterion for electron trapping by an undulating bubble.—We use a simplified model of a positively charged (devoid of electrons) spherical plasma bubble with radius R propagating with uniform velocity v_b [18,36]. A moving-frame Hamiltonian describing plasma electrons' interaction with the bubble is given by $H(\rho, t) = \sqrt{1 + (\mathbf{P} + \mathbf{A})^2} - v_b P_x - \phi$ [18,20,37], where $\rho = (\xi, y, z - z_{\text{osc}})$, $\xi = x - v_b t$, $z_{\text{osc}}(t)$ is the transverse coordinate of the undulating bubble center, \mathbf{P} is the canonical momentum, and \mathbf{A} (ϕ) are the vector (scalar) potentials. Time, length, potential, and electron momentum are normalized to ω_p^{-1} , $k_p^{-1} = c/\omega_p$, $m_e c^2/|e|$, and $m_e c$, respectively, where $\omega_p = \sqrt{4\pi e^2 n_p/m}$ is the electron plasma frequency and n_p is the plasma density.

Under the $A_x = -\phi = \Phi/2$ gauge, we assume that $\Phi = (\rho^2 - R^2)/4$ inside and $\Phi = 0$ outside the bubble [37]. Transverse plasma bubble undulations $z_{\text{osc}}(t) \equiv z_u \cos(\omega_{\text{CEP}} t + \phi_{\text{CEP}})$ excited by the injector pulse introduce time dependence into the Hamiltonian. Here $\omega_{\text{CEP}} \equiv 2\pi/T_{\text{CEP}}$ is the injector CEP slip rate with respect to the bubble speed [28–31,38], z_u is the maximum bubble oscillation amplitude, and $\phi_{\text{CEP}} \equiv \phi_{\text{CEP}}[t(x_0), x_0]$ is the initial CEP evaluated at the time $t(x_0)$ corresponding to the electron's entrance into the bubble at $x = x_0$. Under the relativistic approximation $v_b/c \approx 1 - 1/2\gamma_b^2$ for $\gamma_b \gg 1$, where γ_b is the relativistic factor of the bubble, the undulation period is

$$cT_{\text{CEP}} \approx 2\lambda_{\text{inj}} \left(\frac{1}{\gamma_b^2} + \frac{n_p}{n_{\text{crit}}(\lambda_{\text{inj}})} \right)^{-1}, \quad (1)$$

where $n_{\text{crit}}(\lambda_{\text{inj}}) = \pi m_e c^2 / (e^2 \lambda_{\text{inj}}^2)$ is the critical density for the injector wavelength λ_{inj} .

Electron equations of motion in the x - z plane derived from $H(\rho, t)$ are

$$\begin{aligned} \frac{d\xi}{dt} &= \frac{p_x}{\gamma} - v_b, & \frac{dp_x}{dt} &= -\frac{1}{4} [\xi(1 + v_b) + (v_z - \dot{z}_{\text{osc}})\tilde{z}] \\ \frac{dz}{dt} &= \frac{p_z}{\gamma}, & \frac{dp_z}{dt} &= -\frac{(v_x + 1)\tilde{z}}{4} \end{aligned} \quad (2)$$

where the explicitly time-dependent terms z_{osc} and $\tilde{z}(t) = z - z_{\text{osc}}$ change the Hamiltonian from its initial value of $H(t) = 1$ for the quiescent electrons in front of the bubble. Bubble undulations cause the Hamiltonian to evolve according to $dH/dt = \partial H/\partial t$, enabling some of the plasma electrons to get trapped inside the bubble when the following condition is satisfied:

$$\Delta H = \int dt \dot{p}_z(t) \dot{z}_{\text{osc}}(t) < -1, \quad (3)$$

where the integral is calculated along the electron trajectory [18,20].

To lowest order in the bubble undulation amplitude z_u , and assuming that electron passage time through the bubble $T_{\text{pass}} \sim R$ is much shorter than T_{CEP} , the Hamiltonian increment can be approximated as $\Delta H^{(1)} \approx -z_u \omega_{\text{CEP}} \sin(\phi_{\text{CEP}}) \Delta p^{(0)}$, where $\Delta p^{(0)}$ is the zeroth-order ($z_u = 0$) transverse momentum change of an electron passing through the bubble. For an electron entering the bubble at its edge at $z = \pm R$, the maximum transverse momentum change is $|p_z^{\text{max}}| \approx 0.16R^2$ in the limit $v_b = c$ (See Fig. S1 of the Supplemental Material [39]). Therefore, the trapping condition for an electron entering the bubble's edge at the optimal phase ($\phi_{\text{CEP}} = \pm\pi/2$) is estimated as $z_u > 6/(\omega_{\text{CEP}} R^2)$ in normalized units. Assuming $\omega_{\text{CEP}} \sim \lambda_{\text{inj}} \omega_p^2 / (2\pi c)$ [30], the injection criterion is $z_u > z_u^{\text{tr}}$, where the trapping threshold is $z_u^{\text{tr}}/R \sim 6(k_p R)^{-3} \sqrt{n_{\text{crit}}/n_p}$ in physical units.

PUB-based injection is visualized in Fig. 2(a), where the trajectories given by Eq. (2) are plotted for two initially quiescent electrons. The first (red star: trapped) electron enters the undulating bubble with $\phi_{\text{CEP}} = \pi/2$, while the second (blue star: passing) one is delayed in time, entering the bubble with $\phi_{\text{CEP}} = \pi$. The electrons' initial transverse positions [red star: $z_0 = -R$, blue star: $z_0 = -(R + z_u)$] are chosen such that electrons enter the bubble at its lower edge, and the undulating bubble parameters (see caption) approximately correspond to those of the 3D PIC simulation presented later (Figs. 3 and 4). The trapped electron's Hamiltonian $H(t = 15) < 0$ fulfills the trapping condition $\Delta H < -1$, while the passing electron's Hamiltonian $H(t) > 0$ increases and remains positive. Moreover, the fraction of particles trapped by the bubble rapidly vanishes for $z_u < z_u^{\text{tr}}$ [see Fig. S1(f) of the Supplemental Material [39]]. As this calculation demonstrates, injections occur twice per period: if a bubble traps an electron at (x_1, z_1) for $\phi_{\text{CEP}1}$, then it will also trap a "partner" electron for $\phi_{\text{CEP}2} = \phi_{\text{CEP}1} + \pi$ at $(x_2 = x_1 + v_b T_{\text{CEP}}/2, z_2 = -z_1)$.

To model electron trapping from background plasma, we simulate the interaction of the undulating bubble with a swarm of electrons initially at rest randomly seeded into a 3D volume of initial positions (longitudinal $R < x_0 < 50$ and transverse $-6.5 < y_0, z_0 < 6.5$) entering the bubble during the $0 < t < 200$ time interval. Electron injection occurs every half-period of the bubble oscillation as shown in Fig. 2(b), where electrons are color coded based on their longitudinal injection location x_0 (or, equivalently, injection time $t_0 = x_0/v_b$) with blue injected the earliest and yellow injected the latest. The injected electrons originate from the bubble's edge: since $|\Delta H| \propto z_0^2$ (where z_0 is the impact parameter of an electron entering the bubble),

electrons grazing the bubble at $z_0 \approx R$ are most easily trapped.

The time delay between injections determines the trapped/accelerated electrons's longitudinal structure. As electrons accelerate, they become ultrarelativistic and advance through the bubble. Therefore, the longitudinal spacing between microbunches entering the bubble at the adjacent injection times is $\Delta\xi \approx (c - v_b) \times T_{\text{CEP}}/2 \approx T_{\text{CEP}}/(4\gamma_b^2)$. The resulting modulated injected beam is shown in Figure 2(c), where several ultrashort bunches correspond to different (color-coded) injection times.

Inducing bubble undulations by an NSC pulse.—Next, we establish the optimal wavelength λ_{inj} and duration $\sigma_x \equiv T\lambda_{\text{inj}}$ of the injector pulse with T pulse cycles producing the largest asymmetric plasma flow around the fixed bubble. Flow asymmetry can be used as a proxy for induced bubble undulation amplitude z_u . We use particle swarm simulations similar to those used in Figs. 2(b) and 2(c), except that the bubble is nonundulating, and the electric field of the injector pulse placed ahead of the bubble is given by $E_z = a_{\text{inj}}\omega_{\text{inj}}e^{-(v^2+z^2)}/\sigma_{\text{inj}}^2 e^{-\xi(-R)^2/\sigma_x^2} \times \cos[\omega_{\text{inj}}(x - v_{\text{ph}}t - R) + \phi_{\text{CEP}}]$. Injector

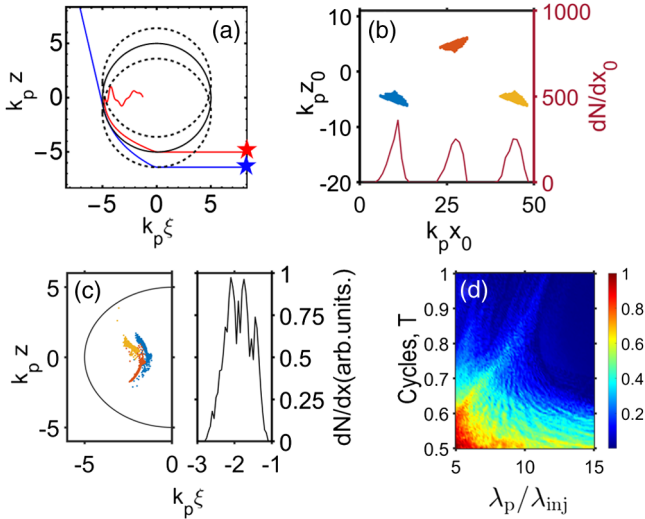


FIG. 2. (a)–(c) Test particle trapping by an undulating bubble and (d) bubble asymmetry by an NSC pulse. (a) Trapped (red, $\phi_{\text{CEP}} = \pi/2$) and passing (blue, $\phi_{\text{CEP}} = \pi$) trajectories for $0 < t < 200$. Bubble boundaries (black lines), unperturbed (solid) and maximally displaced (dashed). (b)–(c) Particle swarm at $t = 200$ from a range of initial conditions (x_0, y_0, z_0) color coded by x_0 . Trapped electrons are plotted in the (x_0, z_0) plane (b) and inside the bubble (c). Red line in (b), density of injected electrons vs their initial position. Black line in (c), longitudinal density. PUB parameters, $k_p R = 5$, $z_u/R = 0.28$, $T_{\text{CEP}} = 35/\omega_p$, $\gamma_b = 5$. (d) Normalized plasma flow asymmetry δz_{ex} (color coded) after passing through the injector pulse and nonoscillating bubble vs NSC wavelength λ_{inj} and pulse cycles $T = \sigma_x/\lambda_{\text{inj}}$.

pulse spot size $\sigma_{\text{inj}} = 3$ and vector potential $a_{\text{inj}} = 4$ are fixed, while the cycle number T and the normalized injector pulse frequency $\omega_{\text{inj}}/\omega_p = \lambda_p/\lambda_{\text{inj}}$ are varied (See the Supplemental Material [39] for details). Each particle is removed from the simulation at the exit time t_{ex} such that $\xi(t_{\text{ex}}) = -R$, and its transverse displacement is $z_{\text{ex}} \equiv z(t_{\text{ex}})$.

Particle-averaged exit transverse displacement $\delta z_{\text{ex}} \equiv \langle z_{\text{ex}} \rangle$ [Fig. 2(d)] is enhanced for (1) longer λ_{inj} and (2) shorter T . While this is unsurprising considering the nonponderomotive scaling $\delta p_z \propto a_0^3 \lambda_{\text{inj}}^2 \sin(\phi_{\text{CEP}})/\sigma_{\text{inj}}^2 T^2$ [30] of the momentum asymmetry, this expression has been derived without the plasma bubble. Owing to the injection threshold scaling $z_u^{\text{tr}} \propto 1/\lambda_{\text{inj}}$, a long-wavelength NSC injector is advantageous for particle trapping.

PIC simulations.—The single-particle model suggests the following sequence of events when a NSC injector pulse copropagates with a strong driver pulse: (i) asymmetric plasma flow around the injector pulse and plasma bubble generated by the driver pulse produces an undulating bubble [Fig. 2(d)], (ii) the latter periodically traps plasma electrons [Fig. 2(b)], and (iii) it produces a structured bunch [Fig. 2(c)]. 3D PIC code VLPL [40] is used to self-consistently model multiple physical effects from the two laser pulses and the plasma, including laser self-guiding [34], depletion of the plasma fields by injected electrons [41], the nonspherical structure of the plasma bubble [42,43], and the deflection of the bubble centroid by the injector pulse. Orthogonally polarized multicycle driver and NSC injector pulses copropagate in tenuous plasma with $n_p = 4.4 \times 10^{18}/\text{cm}^3$; see Fig. 1 for a schematic, Table I for laser parameters, and the Supplemental Material [39] for simulations details. The injector pulse advance $\Delta T = 21$ fs is optimized to inject electrons near the back of the plasma bubble. Because of the low power and short duration, injector pulse energy $U_{\text{inj}} \sim 20$ mJ is a small fraction of the driver pulse energy $U_{\text{dr}} \sim 680$ mJ.

During the early copropagation of the driver and injector pulses [Fig. 3(a)], the former produces the bubble while the latter induces its transverse centroid undulation in the injector polarization direction z . Bubble undulations manifest as a transverse on-axis wakefield $W_{\perp} \equiv E_z + B_y$

TABLE I. Parameters of the driver and injector pulses.

Laser pulse	Driver	Injector 1	Injector 2
Polarization	y	z	z
Wavelength	$\lambda_{\text{dr}} = 0.8 \mu\text{m}$	$\lambda_{\text{inj}} = 2.4 \mu\text{m}$	$\lambda_{\text{inj}}^{(2)} = 1.2 \mu\text{m}$
a_0	3	4	4
FWHM	$T_{\text{dr}} = 22$ fs	$T_{\text{inj}} = 6$ fs	$T_{\text{inj}}^{(2)} = 3$ fs
Spot size	$\sigma_{\text{dr}} = 10 \mu\text{m}$	$\sigma_{\text{inj}} = 8 \mu\text{m}$	$\sigma_{\text{inj}}^{(2)} = 8 \mu\text{m}$
Peak power	$P_{\text{dr}} = 31$ TW	$P_{\text{inj}} = 3.4$ TW	$P_{\text{inj}}^{(2)} = 13.2$ TW

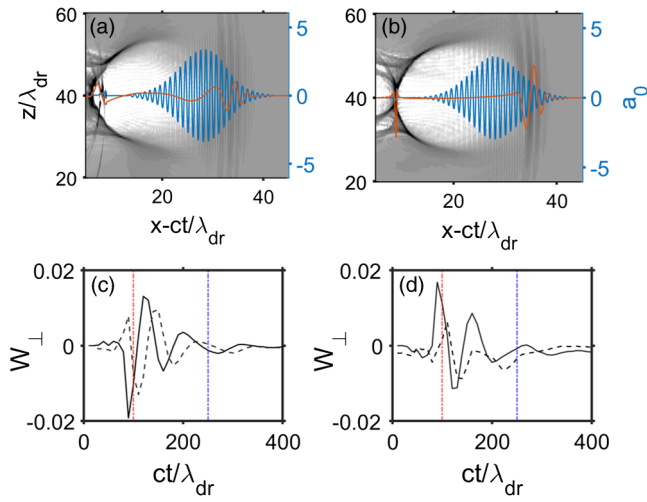


FIG. 3. Evolution of the injector-driver pulses and transverse plasma wakes. (a)–(b) Grayscale, plasma density in the x – z plane around the bubble. Red (blue) lines, on-axis normalized electric fields of the injector (driver) pulses at (a) $x_1 = 0.08$ mm and (b) $x_2 = 0.2$ mm. (c)–(d) On-axis transverse wakes at $\zeta \equiv (x - ct)/\lambda = 9$ [green stars in (a)–(b)]. (c) CEP dependence of W_{\perp} for $\lambda_{\text{inj}} = 2.4 \mu\text{m}$ injector pulse, $\phi_{\text{CEP}} = 0$ (black solid line) and $\phi_{\text{CEP}} = \pi/2$ (black dashed line). (d) Dependence of W_{\perp} on the injector pulse wavelength, $\lambda_{\text{inj}} = 2.4 \mu\text{m}$ (black solid line) and $\lambda_{\text{inj}}^{(2)} = 1.2 \mu\text{m}$ (black dashed line); $\phi_{\text{CEP}} = \pi$ for both wavelengths. Red (blue) dotted-dashed lines, propagation distances x_1 (x_2). All fields scaled to $E_0 = e/mc\omega_{\text{dr}}$. Plasma density, $n_p = 4.4 \times 10^{18} \text{ cm}^{-3}$; laser parameters, see Table I. Simulations, 3D PIC VLPL.

[Fig. 3(c)], where $(E_z, B_y)(\zeta, z = y = 0)$ are the transverse electric-magnetic bubble wakefields. In agreement with Eq. (1), the transverse wake oscillates with period $cT_{\text{CEP}} \approx 70\lambda_{\text{dr}}$ before the injector pulse depletes around $x = L_{\text{inj}}^{\text{depl}} \approx 0.2$ mm. The injector pulse CEP controls the phase of W_{\perp} [Fig. 3(c)]: transverse wakes produced by the injector pulses with the initial values of $\phi_{\text{CEP}} = 0, \pi/2$ are phase shifted by 90° with respect to each other. In contrast, the longitudinal wake $W_{\parallel} \equiv E_x$ is CEP independent [See Fig. S7(b) of the Supplemental Material [39].

The bubble’s radius remains almost constant during the injection process because of our choice of a matched driver laser pulse radius [6] and an extremely short injector pulse. However, we note that when the injector pulse has appreciable amplitude, the back of the bubble where the electrons are injected has a relatively slow phase velocity ($\gamma_b \sim 5$). After the injector depletes, bubble phase velocity increases to a higher value ($\gamma_b \sim 20$). [See Fig S8(d) of the Supplemental Material [39]. The key difference of the described two-pulse scenario with $\lambda_{\text{inj}} \gg \lambda_{\text{dr}}$ from that utilizing a single NSC pulse is the driver pulse dramatically outrunning the injector pulse. The latter rapidly depletes because of its stronger interaction with plasma: $n_{\text{crit}}(\lambda_{\text{inj}}) \ll n_{\text{crit}}(\lambda_{\text{dr}})$. The injector pulse decays after

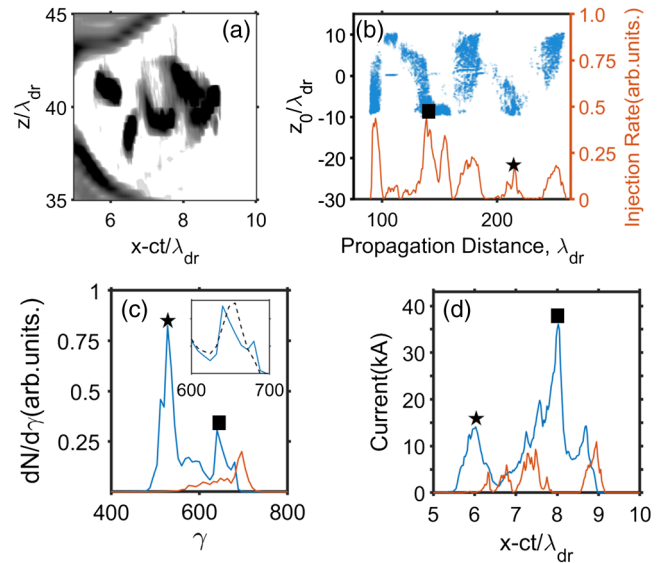


FIG. 4. PUB-based injection/acceleration. (a) Grayscale, density cross section at $x = 0.32$ mm. (b) Electron injection rate (solid line) and injected electrons’ initial transverse positions (blue dots) as a function of propagation distance. (c)–(d) Injected electrons’ energy spectra (c) and current (d) at $x = 1.5$ mm for Injector 1 (blue line) and Injector 2 (red line). Star and square in (b)–(d): the corresponding injection times (b), energy spectra (c), and positions inside the bubble (d). Inset in (c): high-energy spectral peaks at $\phi_{\text{CEP}} = 0$ (solid line) and $\phi_{\text{CEP}} = \pi/2$ (dashed line). Laser parameters, see Table I. Simulations, 3D PIC VLPL.

$L_{\text{inj}}^{\text{depl}} = 250\lambda_{\text{dr}}$ while the driver pulse remains unchanged [Figs. 3(a) and 3(b)]. Injector pulse depletion is mirrored by the transverse plasma wake W_{\perp} decaying over the same distance $L_{\text{inj}}^{\text{depl}}$ marked by the blue dot-dashed line in Fig. 3(c). Therefore, the PUB injection is expected to stop after $x \approx L_{\text{inj}}^{\text{depl}} \ll L_{\text{acc}}$, where $L_{\text{acc}} \approx 1.5$ mm is the acceleration distance determined by driver depletion. Because $L_{\text{acc}} \gg L_{\text{inj}}$, CEP-independent high-energy acceleration is expected.

PIC simulations confirm that a bubble’s centroid undulations trap electrons into the bubble, generating microbunches [Fig. 4(a)]. Several injections with regular spacing $T_{\text{CEP}}/2 \approx 35\lambda/c$ are shown in Fig. 4(b), terminating after $x \approx L_{\text{inj}}^{\text{depl}}$. Consequently, the total injected charge $Q_1 \approx 93$ pC is distributed over several microbunches [Figs. 4(a) and 4(d)]. Electron density peaks are separated by $\Delta\xi \approx T_{\text{CEP}}/4\gamma_b^2 \approx 0.66\lambda_{\text{dr}}$, as estimated earlier. Remarkably, the peak-current spike of $I \approx 36$ kA at $x - ct \approx 8\lambda_{\text{dr}}$ contains $q \approx 25$ pC of charge in a subfemtosecond-scale time interval of $\delta\xi/c \approx 0.8$ fs. Note that this PUB-based injection is caused by transverse bubble undulations, not by the accompanying bubble size modulation [18,20,21] from rapid NSC pulse extinction. This was verified using 2D PIC simulations, where only one (in plane) polarization of the NSC pulse resulted in bubble undulation and electron

injection. The orthogonal polarization produced neither (see Fig. S6 of the Supplemental Material [39]).

The two major current spikes marked as a square and a star in Fig. 4(d) originate from the two correspondingly marked electron injections at $ct_1 \approx 135\lambda_{\text{dr}}$ and $ct_2 \approx 250\lambda_{\text{dr}}$ [Fig. 4(b)]. The current spikes correspond to quasimonoenergetic electron bunches formed after the propagation distance L_{acc} with prominent spectral peaks at $\gamma_1 \approx 630$ (square) and $\gamma_2 \approx 520$ (star) [Fig. 4(c)]. From the inset showing electron energy spectra for $\phi_{\text{CEP}} = 0$ (solid line) and $\phi_{\text{CEP}} = \pi/2$ (dashed line) around γ_1 , we confirm their near CEP independence arising from $L_{\text{acc}} \gg L_{\text{inj}}^{\text{depl}}$. Decoupling between electron acceleration and injection further enables manipulation of the bunch profile using the CEP of the NSC pulse without affecting its energy spectrum [see Fig S4(g) of the Supplemental Material [39]].

The described injection/acceleration approach utilizing a long-wavelength NSC injector was compared to the following scenarios: no injector pulse, short-wavelength ($\lambda_{\text{inj}}^{(2)} = \lambda_{\text{inj}}/2$) injector pulse with $P_{\text{inj}}^{(2)} = 4P_{\text{inj}} = 13.2$ TW, and $\tau = 3$ fs. While the injector pulse alone can also inject-accelerate electrons, it cannot sustain a stable accelerating bubble over a significant [28,29,31] distance, resulting in an energy gain of less than 10 MeV and charge less than $q \approx 16$ pC. No injector scenario yields a small charge $q \approx 1$ pC, because the slowly evolving driver pulse cannot efficiently inject electrons. A short-wavelength injector scenario, preserving the injector pulse's ponderomotive potential $U_p \propto P_{\text{inj}}\lambda_{\text{inj}}^2/\sigma_{\text{inj}}^2$ while reducing its wavelength, also results in inefficient injection. The corresponding current profile is indicated by a red line in Fig. 4(d), and the total charge $Q_2 \approx 21$ pC $\ll Q_1$ [Fig. 4(c)]. This is because the nonponderomotive scaling of the injector-induced bubble undulation favors longer injector wavelengths [Fig. 2(d)]. The smaller bubble undulation amplitude is evidenced by the smaller W_{\perp} amplitude [dashed line in Fig. 3(d) for $\lambda_{\text{inj}}^{(2)}$] compared with the λ_{inj} case (solid line).

In conclusion, we propose and theoretically demonstrate a two-pulse CEP-controlled scheme for injecting and accelerating electrons from a preformed plasma. We combine a near-single-cycle long-wavelength laser pulse for rapid electron injection with a multicycle short-wavelength driver pulse for long-distance acceleration of the injected electrons to generate subfemtosecond high-current (tens of kA) electron microbunches with ultra-relativistic energies (hundreds of MeVs). Such beams can be used as a compact source of ultrashort x-ray radiation owing to their high-energy and large-amplitude betatron motion.

This work was supported by the Department of Energy under a Grant No. DE-SC0019431 and by the National Science Foundation under a Grant No. PHY-2109087. The

authors thank the Texas Advanced Computing Center (TACC) at The University of Texas at Austin for providing the HPC resources.

- [1] V. Malka, J. Faure, Y. A. Gauduel, E. Lefebvre, A. Rousse, and K. T. Phuoc, Principles and applications of compact laser-plasma accelerators, *Nat. Phys.* **4**, 447 (2008).
- [2] S. M. Hooker, Developments in laser-driven plasma accelerators, *Nat. Photonics* **7**, 775 (2013).
- [3] E. Esarey, C. B. Schroeder, and W. P. Leemans, Physics of laser-driven plasma-based electron accelerators, *Rev. Mod. Phys.* **81**, 1229 (2009).
- [4] K. Nakamura, B. Nagler, C. T'oth, C. G. R. Geddes, C. B. Schroeder, E. Esarey, and W. P. Leemans, GeV electron beams from a centimeter-scale channel guided laser wakefield accelerator, *Phys. Plasmas* **14**, 056708 (2007).
- [5] X. Wang *et al.*, Quasi-monoenergetic laser-plasma acceleration of electrons to 2 GeV, *Nat. Commun.* **4**, 1988 (2013).
- [6] W. Lu, M. Tzoufras, C. Joshi, F. S. Tsung, W. B. Mori, J. Vieira, R. A. Fonseca, and L. O. Silva, Generating multi-GeV electron bunches using single stage laser wakefield acceleration in a 3D nonlinear regime, *Phys. Rev. ST Accel. Beams* **10**, 061301 (2007).
- [7] W. P. Leemans, A. J. Gonsalves, H.-S. Mao, K. Nakamura, C. Benedetti, C. B. Schroeder, C. T'oth, J. Daniels, D. E. Mittelberger, S. S. Bulanov, J.-L. Vay, C. G. R. Geddes, and E. Esarey, Multi-GeV Electron Beams from Capillary-Discharge-Guided Subpetawatt Laser Pulses in the Self-Trapping Regime, *Phys. Rev. Lett.* **113**, 245002 (2014).
- [8] H. T. Kim, V. B. Pathak, K. H. Pae, A. Lifschitz, F. Sylla, J. H. Shin, C. Hojibota, S. Ku. Lee, J. H. Sung, H. W. Lee, E. Guillaume, C. Thauray, K. Nakajima, J. Vieira, L. O. Silva, V. Malka, and C. H. Nam, Stable multi-GeV electron accelerator driven by waveform-controlled PW laser pulses, *Sci. Rep.* **7**, 10203 (2017).
- [9] A. J. Gonsalves *et al.*, Petawatt Laser Guiding and Electron Beam Acceleration to 8 GeV in a Laser-Heated Capillary Discharge Waveguide, *Phys. Rev. Lett.* **122**, 084801 (2019).
- [10] C. B. Schroeder, E. Esarey, C. G. R. Geddes, C. Benedetti, and W. P. Leemans, Physics considerations for laser-plasma linear colliders, *Phys. Rev. ST Accel. Beams* **13**, 101301 (2010).
- [11] H.-S. Park *et al.*, High-energy *K α* radiography using high-intensity, short-pulse lasers, *Phys. Plasmas* **13**, 056309 (2006).
- [12] S. Kneip, S. R. Nagel, C. Bellei, N. Bourgeois, A. E. Dangor, A. Gopal, R. Heathcote, S. P. D. Mangles, J. R. Marques, A. Maksimchuk, P. M. Nilson, K. T. Phuoc, S. Reed, M. Tzoufras, F. S. Tsung, L. Willingale, W. B. Mori, A. Rousse, K. Krushelnick, and Z. Najmudin, Observation of Synchrotron Radiation from Electrons Accelerated in a Petawatt-Laser-Generated Plasma Cavity, *Phys. Rev. Lett.* **100**, 105006 (2008).
- [13] D. J. Stark, T. Toncian, and A. V. Arefiev, Enhanced Multi-MeV Photon Emission by a Laser-Driven Electron Beam in a Self-Generated Magnetic Field, *Phys. Rev. Lett.* **116**, 185003 (2016).
- [14] M. Schollmeier, A. B. Sefkow, M. Geissel, A. V. Arefiev, K. A. Flippo, S. A. Gaillard, R. P. Johnson, M. W. Kimmel,

- D. T. Offermann, P. K. Rambo, J. Schwarz, and T. Shimada, Laser-to-hot-electron conversion limitations in relativistic laser matter interactions due to multipicosecond dynamics, *Phys. Plasmas* **22**, 043116 (2015).
- [15] I. Pomerantz, E. McCary, A. R. Meadows, A. Arefiev, A. C. Bernstein, C. Chester, J. Cortez, M. E. Donovan, G. Dyer, E. W. Gaul, D. Hamilton, D. Kuk, A. C. Lestrade, C. Wang, T. Ditmire, and B. M. Hegelich, Ultrashort Pulsed Neutron Source, *Phys. Rev. Lett.* **113**, 184801 (2014).
- [16] H. Chen, A. Link, Y. Sentoku, P. Audebert, F. Fiuza, A. Hazi, R. F. Heeter, M. Hill, L. Hobbs, A. J. Kemp, G. E. Kemp, S. Kerr, D. D. Meyerhofer, J. Myatt, S. R. Nagel, J. Park, R. Tommasini, and G. J. Williams, The scaling of electron and positron generation in intense laser-solid interactions, *Phys. Plasmas* **22**, 056705 (2015).
- [17] P. Mora and T. M. Antonsen, Jr., Kinetic modeling of intense, short laser pulses propagating in tenuous plasmas, *Phys. Plasmas* **4**, 217 (1997).
- [18] S. Kalmykov, S. A. Yi, V. Khudik, and G. Shvets, Electron Self-Injection and Trapping into an Evolving Plasma Bubble, *Phys. Rev. Lett.* **103**, 135004 (2009).
- [19] R. Lehe, A. F. Lifschitz, X. Davoine, C. Thaur, and V. Malka, Optical Transverse Injection in Laser-Plasma Acceleration, *Phys. Rev. Lett.* **111**, 085005 (2013).
- [20] S. A. Yi, V. Khudik, S. Y. Kalmykov, and G. Shvets, Hamiltonian analysis of electron self-injection and acceleration into an evolving plasma bubble, *Plasma Phys. Controlled Fusion* **53**, 014012 (2011).
- [21] A. J. Gonsalves *et al.*, Tunable laser plasma accelerator based on longitudinal density tailoring, *Nat. Phys.* **7**, 862 (2011).
- [22] M. Chen, Z. M. Sheng, Y. Y. Ma, and J. Zhang, Electron injection and trapping in a laser wakefield by field ionization to high-charge states of gases, *J. Appl. Phys.* **99**, 056109 (2006).
- [23] A. Pak, K. A. Marsh, S. F. Martins, W. Lu, W. B. Mori, and C. Joshi, Injection and Trapping of Tunnel-Ionized Electrons into Laser-Produced Wakes, *Phys. Rev. Lett.* **104**, 025003 (2010).
- [24] C. McGuffey, A. G. R. Thomas, W. Schumaker, T. Matsuoka, V. Chvykov, F. J. Dollar, G. Kalintchenko, V. Yanovsky, A. Maksimchuk, K. Krushelnick, V. Yu. Bychenkov, I. V. Glazyrin, and A. V. Karpeev, Ionization Induced Trapping in a Laser Wakefield Accelerator, *Phys. Rev. Lett.* **104**, 025004 (2010).
- [25] X. L. Xu, C.-H. Pai, C. J. Zhang, F. Li, Y. Wan, Y. P. Wu, J. F. Hua, W. Lu, W. An, P. Yu, C. Joshi, and W. B. Mori, Nanoscale Electron Bunching in Laser-Triggered Ionization, *Phys. Rev. Lett.* **117**, 034801 (2016).
- [26] A. F. Lifschitz and V. Malka, Optical phase effects in electron wakefield acceleration using few-cycle laser pulses, *New J. Phys.* **14**, 053045 (2012).
- [27] M. Ouillé *et al.*, Relativistic-intensity near-single-cycle light waveforms at kHz repetition rate, *Light Sci. Appl.* **9**, 47 (2020).
- [28] J. Huijts, I. Andriyash, L. Rovige, A. Vernier, and J. Faure, Identifying observable carrier-envelope phase effects in laser wakefield acceleration with near-single-cycle pulses, *Phys. Plasmas* **28**, 043101 (2021).
- [29] S. Xu, J. Zhang, N. Tang, S. Wang, W. Lu, and Z. Li, Periodic self-injection of electrons in a fewcycle laser driven oscillating plasma wake, *AIP Adv.* **10**, 095310 (2020).
- [30] E. N. Nerush and I. Yu. Kostyukov, Carrier-Envelope Phase Effects in Plasma-Based Electron Acceleration with Few-Cycle Laser Pulses, *Phys. Rev. Lett.* **103**, 035001 (2009).
- [31] F. Salehi, M. Le, L. Railing, M. Kolesik, and H. M. Milchberg, Laser-Accelerated, Low Divergence 15 MeV Quasi-Monoenergetic Electron Bunches at 1 kHz, *Phys. Rev. X* **11**, 021055 (2021).
- [32] J. Faure, D. Gustas, D. Guénot, A. Vernier, F. Böhle, M. Ouillé, S. Haessler, R. Lopez-Martens, and A. Lifschitz, A review of recent progress on laser-plasma acceleration at kHz repetition rate, *Plasma Phys. Controlled Fusion* **61**, 014012 (2019).
- [33] S. Chou, J. Xu, D. Cardenas, D. Rivas, T. Wittmann, F. Krausz, S. Karsch, and L. Veisz, Sub-2-cycle laser-driven wakefield electron acceleration, in *Proceedings of the 2013 Conference on Lasers and Electro-Optics—International Quantum Electronics Conference* (IEEE, New York, 2013), p. 1, <https://dx.doi.org/10.1109/CLEOE-IQEC.2013.6801138>.
- [34] P. Sprangle, E. Esarey, J. Krall, and G. Joyce, Propagation and Guiding of Intense Laser Pulses in Plasmas, *Phys. Rev. Lett.* **69**, 2200 (1992).
- [35] O. Lundh, J. Lim, C. Rechatin *et al.*, Few femtosecond, few kiloampere electron bunch produced by a laser-plasma accelerator, *Nat. Phys.* **7**, 219 (2011).
- [36] I. Kostyukov, A. Pukhov, and S. Kiselev, Phenomenological theory of laser-plasma interaction in “bubble” regime, *Phys. Plasmas* **11**, 5256 (2004).
- [37] I. Yu. Kostyukov, E. N. Nerush, A. Pukhov, and V. Seredov, Electron Self-Injection in Multidimensional Relativistic-Plasma Wake Fields, *Phys. Rev. Lett.* **103**, 175003 (2009).
- [38] Y. Ma, L. Chen, D. Li, W. Yan, K. Huang, M. Chen, Z. Sheng, K. Nakajima, T. Tajima, and J. Zhang, Generation of femtosecond gamma-ray bursts stimulated by laser-driven hosing evolution, *Sci. Rep.* **6**, 30491 (2016).
- [39] See Supplemental Material at <http://link.aps.org/supplemental/10.1103/PhysRevLett.127.164801> for discussion of injection condition, discussion on non-ponderomotive scaling, effect of changing injector pulse, difference in time scale between the injector and driver pulse, overall emittance of whole beam versus overall emittance of individual beam, confirmation of necessity of oscillation for injection using 2D simulation, simulation details, independent control of longitudinal and transverse wakes by near single cycle pulse, and impact of near single cycle pulse on plasma bubble formation and evolution.
- [40] A. Pukhov, Three-dimensional electromagnetic relativistic particle-in-cell code VLPL (Virtual Laser Plasma Lab), *J. Plasma Phys.* **61**, 425 (1999).
- [41] M. Tzoufras, W. Lu, F. S. Tsung, C. Huang, W. B. Mori, T. Katsouleas, J. Vieira, R. A. Fonseca, and L. Silva, Beam loading by electrons in nonlinear plasma wakes, *Phys. Plasmas* **16**, 056705 (2009).
- [42] W. Lu, C. Huang, M. Zhou, W. B. Mori, and T. Katsouleas, Nonlinear Theory for Relativistic Plasma Wakefields in the Blowout Regime, *Phys. Rev. Lett.* **96**, 165002 (2006).
- [43] S. A. Yi, V. Khudik, C. Siemon, and G. Shvets, Analytic model of electromagnetic fields around a plasma bubble in the blow-out regime, *Phys. Plasmas* **20**, 013108 (2013).